JLAB-TN-02-041
24 September 2002

DC Field Quality Characterization of FEL Upgrade Dipoles

D. Douglas and *G. Biallas*

Abstract

We review modeling results (provided by Schultheiss [1]) that characterize field quality in FEL Upgrade Endloop GX, GQ, and GY dipoles. These results are compared to specification and potential discrepancies addressed. We find that adjustment of the GX and GQ lengths and GY gap to appropriately selected values, possibly coupled with judicious (but only eventual) use of length shims on the GX and GQ, will likely provide operationally adequate performance from all three types of magnet as they are presently designed.

Introduction

Successful operation of the FEL Upgrade will require endloop dipoles meeting stringent field quality specifications [2] across the full machine dynamic range of 80 to 210 MeV/c. These specifications [3] address the accuracy, reproducibility, and local variability in magnet core field and field integral, and are summarized in Table 1. Accuracy in field integral insures that the beam will experience properly executed bend angles during recirculation; accuracy in core field insures that bend radii will match design, yielding a properly focused beam. Flatness (limitation of transverse variability) in core field and field integral ensures that phase space distortion (with associated emittance dilution and halo generation) will be avoided. Reproducibility is required to allow machine restoration.

Table 1: Summary Specifications for Endloop Dipoles

Parameter	Beam Manifestation	Error Specification	
Field Integral	bend angle	GX, GQ GY	10^{-3} relative error $¼ \times 10^{-3}$ relative error
Core Field	bend radius, focusing effects	GX, GQ GY	10^{-3} relative error $¼ \times 10^{-3}$ relative error
Field Integral & Core Field Flatness	phase space distortion, emittance dilution	GX,GQ,GY	10^{-4} relative error
Reproducibility	orbit, focusing errors during restoration	GX,GQ,GY	10^{-4} relative error

Several aspects of GY design geometry and numerically modeled field quality are discussed elsewhere [4]. In the following, we document the GX and GQ design geometry and compare numerical modeling results for the GX, GQ and GY designs to specification. Where discrepancies are noted, we discuss operationally practical methods for bringing all designs into compliance with specification.

Reverse Bend Geometry

Both IR and UV drive beams traverse GQ and GX dipoles as shown in Figure 1. In addition, the UV drive beam traverses a subset of the GX dipoles with a geometry to be discussed below. The beam transport system design uses the bend angle θ, radius ρ, and pole face rotations ϕ to characterize the magnet. In this context, entry and exit are symmetrical.

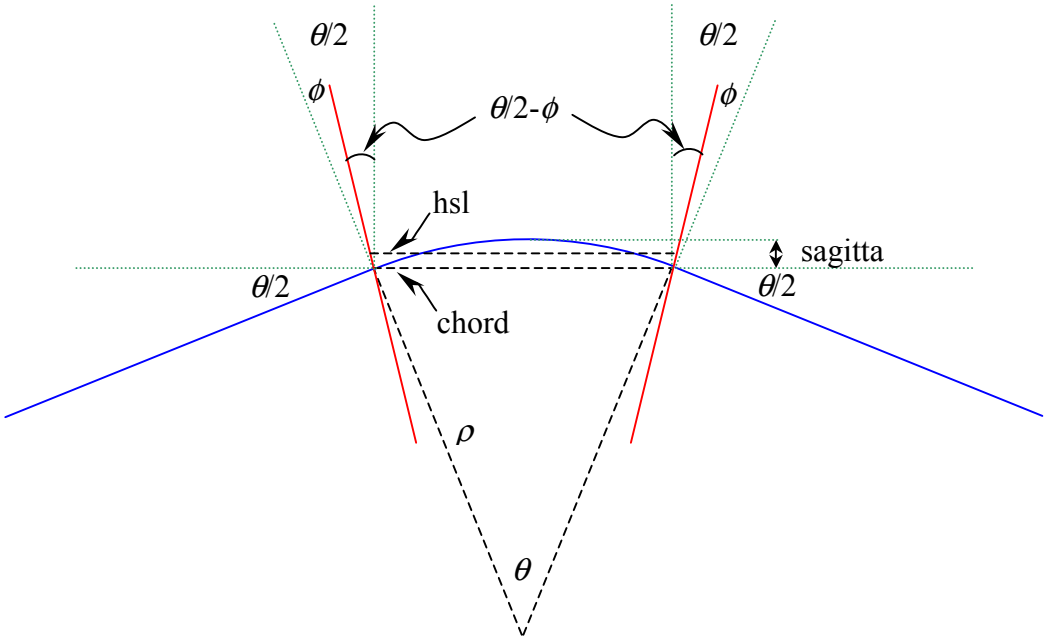

Figure 1: GQ/GX geometry employed in IR and some UV applications. Beam trajectory is shown in blue; effective pole locations are solid red, primary magnet characteristics (chord, half sagitta line, radii) are dashed black, and reference lines are dotted green.

To facilitate comparison to magnetic modeling and measurement, field integrals along various axes parallel to the chord of the circular arc subtended by the trajectory must be computed. Mechanical engineering and design is most conveniently accommodated by using as a reference the axis laterally centered between the chord of the orbit and the mid-point of the circular arc of the beam trajectory; as it is displaced from either location by half the sagitta, we denote this reference axis as the "half-sagitta line" (hsl). The following expressions characterize the parameters of interest – sagitta, chord length, and the length $L(d)$ of line a segment offset by a specified amount d from the reference half sagitta line.

Sagitta: $s = \rho\,(1 - \cos\,\theta/2)$

Chord length: $L_{chord} = 2\rho \sin\,\theta/2$

Length of hsl: $L_{hsl} = L_{chord} + 2\,(s/2) \tan\,(\theta/2-\phi)$
$= 2\rho \sin\,\theta/2 + s \tan\,(\theta/2-\phi)$

Length of line offset by d from hsl:

$L(d) = L_{hsl} + 2\,d \tan\,(\theta/2-\phi)$
$= 2\rho \sin\,\theta/2 + s \tan\,(\theta/2-\phi) + 2\,d \tan\,(\theta/2-\phi)$

The core field of the magnet at an operating momentum p (MeV/c) is selected to provide a 1.2 m bend radius. Given the beam rigidity $B\rho$ of 0.0333564095198 kg-m/(MeV/c), the required operating field is (with p in MeV/c)

$$B = B\rho/\rho = 0.0333654095198 \text{ kg-m} \times p \,/\, 1.2 \text{ m} = 0.0277970079331667\, p \text{ kg-m} .$$

The design field integral along an axis offset by d from the half sagitta line is then $BL(d)$. This will be compared to the results of magnetic modeling at various momenta and for a variety of offsets in both the GX and GQ.

GX UV Geometry

One pair of GX dipoles – those on the backleg axis – are used to direct beam to and from the UV bypass. This is accomplished by switching out half the coil package (dropping the number of excited turns), reducing the total magnet drive current by a factor of two and thus halving the core field. The orbit radius then becomes double the nominal value – 2.4 m rather than 1.2 m. Figure 2 presents the geometry. As the beam no longer moves symmetrically through the magnet, the entry and exit pole face rotation angles are not equal, and the beam crosses the exit pole obliquely. The lower core field and altered geometry result in a bend angle approximately, though not exactly, half that in the IR geometry.

The UV bend angle θ_{UV} is readily obtained from the IR angle θ_{IR} by noting that the doubling of the bend radius leads to a geometry with a number of identical triangles, as indicated in Figure 2. The IR orbit described by Figure 1 dictates that the angle between the pole and the vertical be $\theta_{IR}/2-\phi$. The triangle defined by the exit point of the IR orbit, the exit point of the UV orbit, and the center of the UV orbit can then be characterized by the law of sines to determine the UV bend angle. Specifically,

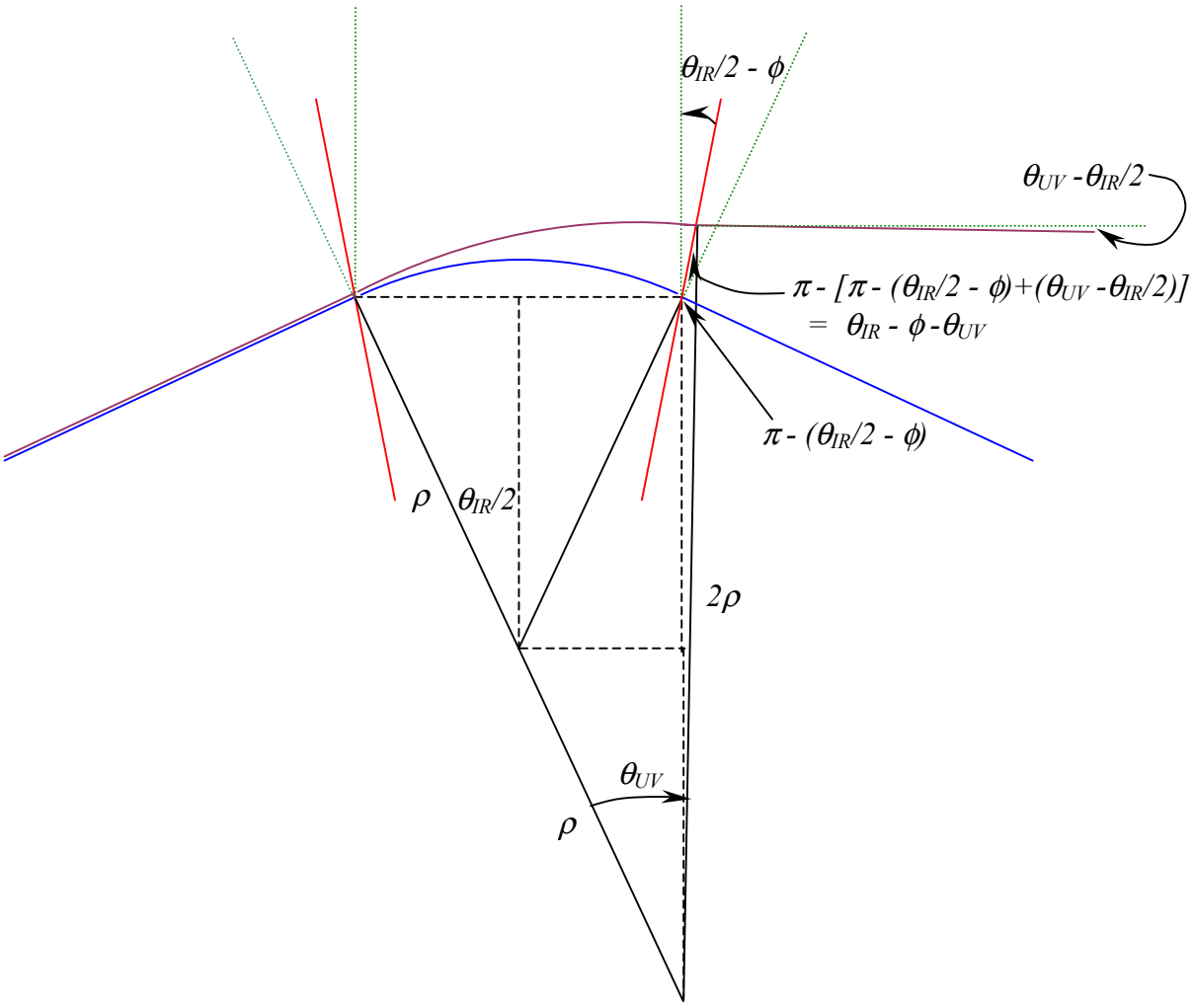

Figure 2: UV orbit geometry; GX excitation is half of nominal IR value. Blue trajectory – nominal IR trajectory; purple trajectory – UV beam; black – IR/UV orbit geometry; green – reference geometry.

$$\frac{2\rho}{\sin\left(\pi-\left(\frac{\theta_{IR}}{2}-\phi\right)\right)}=\frac{2\rho\cos\left(\frac{\theta_{IR}}{2}\right)}{\sin\left(\theta_{IR}-\phi-\theta_{UV}\right)}$$

The UV angle is therefore specified by the following expression.

$$\theta_{UV}=\theta_{IR}-\phi-\sin^{-1}\left\{\cos\left(\frac{\theta_{IR}}{2}\right)\sin\left(\frac{\theta_{IR}}{2}-\phi\right)\right\}$$

For the Upgrade GX ($\theta_{IR} = 43.383565^{o}$, $\phi = 2^{o}$), this yields $\theta_{UV} = 23.1374996188^{o}$.

Additional parameterization and the associated reference geometry for engineering design and numerical simulation are addressed by Figures 3 and 4. Figure 3 characterizes the entry and exit angles of the UV orbit and provides the orientation of the chord of the UV orbit. Engineering and magnetic modeling refer to the half-sagitta line, also shown, which runs parallel to the chord. The lengths of this reference line and test axes offset from it are evaluated using information in Figure 4.

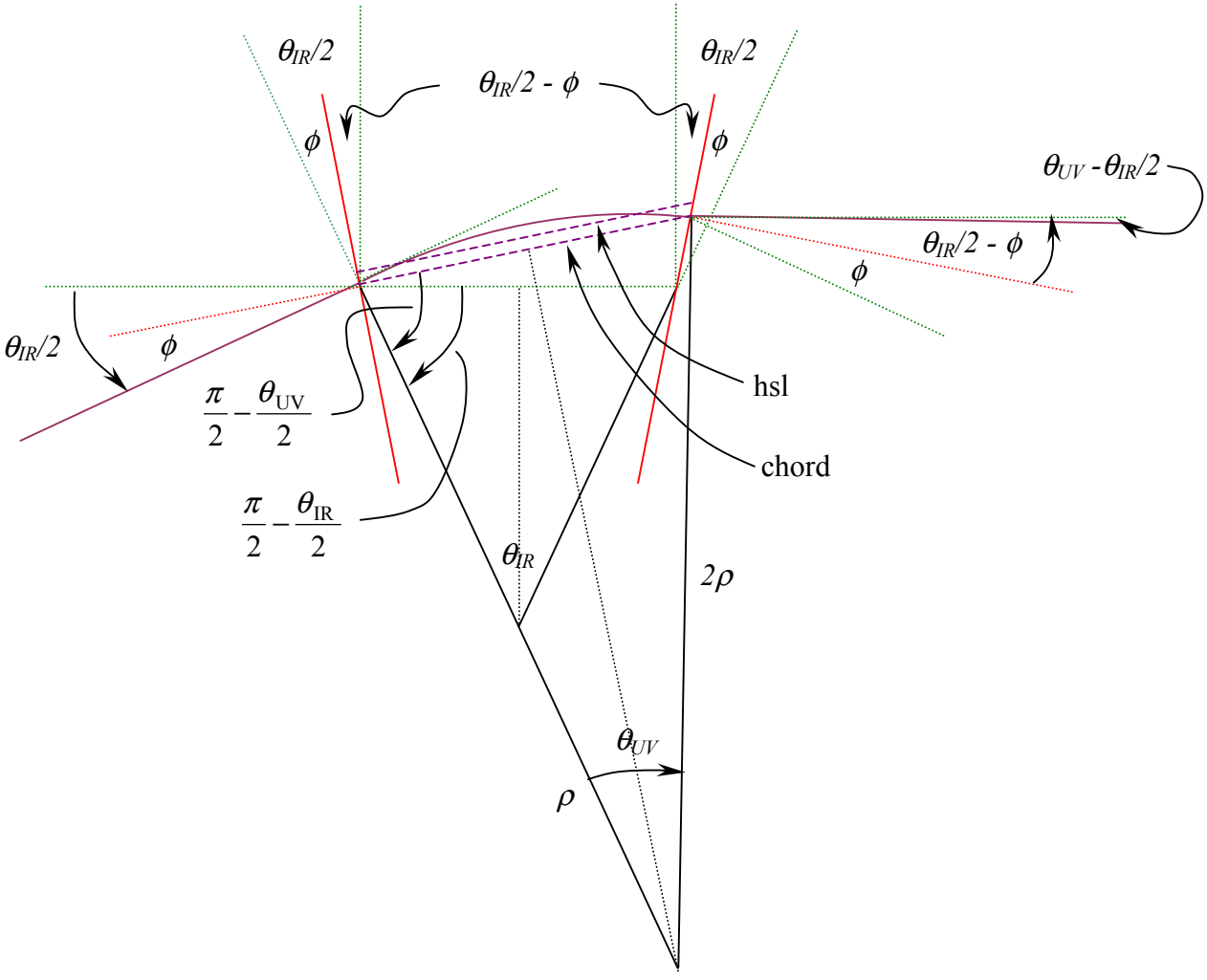

Figure 3: Geometry of UV orbit through GX dipole.

Inspection of Figure 3 provides the following information.

Entrance pole face rotation angle:	ϕ
Exit pole face rotation angle:	$\theta_{UV} - \theta_{IR}/2 - (\theta_{IR}/2 - \phi) = \theta_{UV} - \theta_{IR} + \phi$
Angle of chord and hsl relative to horizontal:	$(\pi/2 - \theta_{UV}/2) - (\pi/2 - \theta_{IR}/2) = \theta_{IR}/2 - \theta_{UV}/2$
Length of chord:	$L_{chord} = 4\rho \sin \theta_{UV}/2$
Sagitta:	$s = 2\rho (1 - \cos \theta_{UV}/2)$

The latter results follow from the fact that the radius of the UV orbit is 2ρ. Figure 4 allows us to evaluate the length of the hsl and any selected offset axis. The chord is shown as a dashed purple line; a test line offset by d is similarly presented. χ_1 and χ_2 denote respectively the angles between the entrance and exit pole faces and the perpendiculars to the chord. These are readily established given the information in Figure 3, which provides the angle between the chord and the horizontal (and thus the angle between the perpendicular to the chord and the vertical. For χ_1, we note

$$\chi_1 + \theta_{IR}/2 - \theta_{UV}/2 = \theta_{IR}/2 - \phi$$

So that

$$\chi_1 = \theta_{UV}/2 - \phi$$

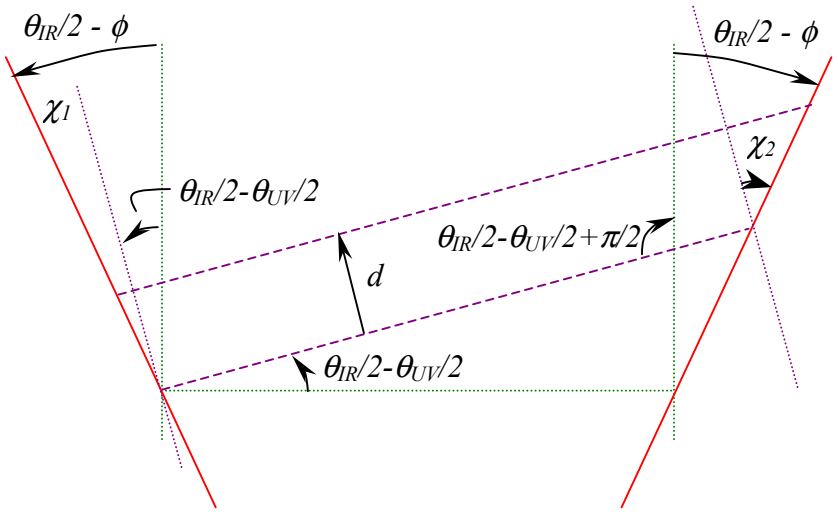

Figure 4: Geometry of UV mechanical reference lines.

Similarly, for χ_2 we note

$$\chi_2 + \pi/2 = (\theta_{IR}/2 - \theta_{UV}/2 + \pi/2) + (\theta_{IR}/2 - \phi)$$

so that

$$\chi_2 = \theta_{IR} - \theta_{UV}/2 - \phi .$$

The length of a line offset by $d_{from\ chord}$ from the chord will then be

$$L\ (d_{from\ chord}) = L_{chord} + d_{from\ chord} \tan \chi_1 + d_{from\ chord} \tan \chi_2$$

In particular, the lengths of the hsl and a test line offset by d from the hsl will be as follows.

$$L_{hsl} = L_{chord} + (s/2)\ (\tan \chi_1 + \tan \chi_2) = 4\ \rho \sin \theta_{UV}/2 + (s/2)\ (\tan \chi_1 + \tan \chi_2)$$

$$L(d) = L_{hsl} + d(\tan \chi_1 + \tan \chi_2) = 4\ \rho \sin \theta_{UV}/2 + (d + s/2)\ (\tan \chi_1 + \tan \chi_2)$$

In the following, we will use these expressions to evaluate the nominal or "design" field integral along multiple test axes through the GX and GQ dipoles. The values so derived will be compared to the results of numerical modeling provided by Schultheiss [1].

Dipole Field Characterization

Magnetic performance of the GX, GQ and GY dipoles has been simulated in some detail by Tom Schultheiss of AES [1]. Some of the GY results have been discussed elsewhere [4]. To certify the magnet designs under consideration, core field accuracy and homogeneity throughout the working aperture of the magnet must be examined. In addition, the value of the field integral along the hsl and its uniformity around that line must be characterized. This must be done at excitations spanning the 80-210 MeV/c operating range of the recirculator. The following data was therefore generated by simulation

GQ [5]: the operating current required to produce the design core field at 80, 145, 190 and 210 MeV/c was established

at 80, 145, and 210 MeV/c, the homogeneity of the core field was evaluated

at 80, 145, and 210 MeV/c, the field integrals along the hsl and a number of displaced axes parallel to it were evaluated. The "effective length" of

the magnet – the field integral divided by the core field – was thereby established.

GX [6,7]: the above simulations were performed around the IR orbit, and, in addition,

the operating current required to produce the UV design core field at 145 and 210 MeV/c was evaluated

at the two UV currents, the homogeneity of the core field was evaluated

at the two UV currents, the field integrals along the UV hsl and a number of displaced axes parallel to it were evaluated. The "effective length" of the magnet – the field integral divided by the core field – was thereby established.

GY [8]: the operating current required to produce the design core field at 80, 145, and 210 MeV/c was established

at 80, 145, and 210 MeV/c, the homogeneity of the core field was examined

at 80, 145, and 210 MeV/c, the field integrals along the central (1 m radius) trajectory and a set of radially displaced trajectories, were evaluated. The "effective length" of the magnet – the field integral divided by the core field – was thereby established.

Comparison of the currents required by the various magnets at different operating momenta will characterize the tracking accuracy – how well the dipoles match when operated at a common current (on the buss). Comparison of the "effective length" to the design values dictated by the expressions established above will further characterize the tracking accuracy and will indicate if the designs suffer unduly from saturation effects.

Accuracy in Core Field and Field Integral; Tracking Accuracy

Table 2 presents the IR orbit "design" values for core field at each operating momentum, and the effective length - at half-sagitta for the reverse bends and along the nominal 1 m radius orbit for the π-bend – which is nominally momentum independent. It also presents the corresponding values from simulation. We note that the core fields were, in simulation, set by adjusting the simulated magnet operating current; as a result the core fields closely match design values, but at differing currents. In practice, the machine will be operated by setting the dipole buss while "turning the first corner" – that is, by adjusting the buss current until the first bend is properly executed. We therefore list the relative deviation of GQ and GY operating current from that of the GX. In the case of the

GY, "half-sagitta lengths" are replaced by the corresponding circular arc length. In each case, the simulated effective length is defined as the field integral along the design reference path (either hsl or circular arc) divided by the core field.

Table 2: Comparison of design and modeled fields, field integrals (along hsl) and currents, at various operating momenta (MeV/c)

Property	GX				GQ				GY		
momentum (MeV/c)	80	145	190	210	80	145	190	210	80	145	210
design field (kg)	2.2238	4.0306	5.2814	5.8374	2.2238	4.0306	5.2814	5.8374	2.6685	4.8367	7.0048
design length (m)	0.9175				0.8948				3.1416		
design ∫Bdl (kg-m)	2.0403	3.6980	4.8456	5.3557	1.9898	3.6065	4.7258	5.2232	8.3834	15.1949	22.0064
simulated field (kg)	2.2238	4.0306	5.2818	5.8371	2.2236	4.0302	5.2814	5.8372	2.6686	4.8369	7.0052
required current (A)	85.1675	154.4485	203.4903	227.2750	84.9770	154.1385	203.1293	227.2750	84.8408	153.8040	223.8659
$(I-I_{GX})/I_{GX}$					*-0.0022*	*-0.0020*	*-0.0018*	*0*	*-0.0038*	*-0.0042*	*-0.0150*
simulated ∫Bdl (kg-m)	2.0512	3.7152	4.8607	5.3562	2.0012	3.6244	4.7417	5.2235	8.3806	15.1903	22.0096
$(\int Bdl-\int Bdl_{design})/\int Bdl_{design}$	*0.0053*	*0.0047*	*0.0031*	*0.0001*	*0.0057*	*0.0050*	*0.0034*	*0.0001*	*-0.0003*	*-0.0003*	*0.0001*
effective length (m)	0.9224	0.9217	0.9203	0.9176	0.9000	0.8993	0.8978	0.8949	3.1404	3.1405	3.1419
$(L_{effective}-L_{design})/L_{design}$	*0.0053*	*0.0046*	*0.0031*	*0.0001*	*0.0058*	*0.0050*	*0.0034*	*0.0001*	*-0.0003*	*-0.0004*	*0.0001*

Inspection of Table 2 reveals important features of magnet behavior. First, it is possible to get very good agreement between the design and simulated core fields (order 0.1 ppt), but the currents required to do so vary significantly amongst the magnets. This was expected in the GY at 210 MeV/c – shunts are provided to accommodate this – but it was not anticipated in the GQ at lower excitation (where the deviation, 2 ppt, will put the core field a factor of 2 out of spec when running at the current that is operationally defined by the GX). Similarly, the shunt is "running out of range" in the GY at the lower excitations, tracking the GX current uncomfortably closely (4 ppt, rather than the design offset of 1.5%).

Secondly, though the core field matches design rather closely, at lower momenta the GX and GY field integrals along the hsl significantly exceed the design values (at ~0.5%, or 5 times the Table 1 specification). These magnets therefore, in effect, appear "too long" at below full excitation. This is not the case for the GY, in which the deviation of $\lesssim$0.3 ppt essentially matches specification (¼ ppt).

This combination of current mismatch and effective length error at low excitation suggests that the magnets, which were designed at 210 MeV/c and simply checked at lower excitation – run somewhat saturated at the top end. This is not a problem, provided that the saturation effects do not adversely affect field homogeneity (we shall see below that they do not) and provided we can develop a means of correcting the current and field integral mismatch that will bring all relevant parameters into compliance with specification and that will be operationally tractable.

A potential scenario – shave, shunt, shim – would have us shave ~5 mm off the length of the GX and GQ, shunt a fraction of the GQ operating current, and then shim both the GX and GQ lengths for operation at high momentum. This solution, though quantitatively

acceptable, has unpleasant operational implications. First, the use of a GQ shunt will complicate machine operation by requiring setup and restoration of an additional "knob" in a location that is already rather underconstrained. Secondly, shimming for the highest momenta will impose invasive operating conditions during energy changes (and potentially during switching between IR to UV). Thirdly, this scenario does not address the apparent saturation of the GY, which leads to a reduction of the required shunt from the design of 1.5% at 210 MeV/c to less than ½% at 80-145 MeV/c. The potential need for "adders" thus becomes a concern.

As an alternative, we have investigated the global optimization of fields and field integrals in all three magnet types as a function of parameters that can be controlled within the present design scope: the GX and GQ magnet length, buss current, the GY shunt current, the GY gap, and GX and GQ shim lengths. "Rules of engagement" for this optimization were as follows:

1) It proceeded in a manner that is consistent with machine operation. For this reason,
   a) the buss current was used at each of four momentum set points (80, 145, 190, and 210 MeV/c) to set the GX field integral – this will "turn the corner" and thereby properly set the bend angle into the endloop;
   b) the GY shunt current was used to set the GY field – this insured the orbit radius through the π-bend was correct and that the beam would thereby be centered in the trim quads up- and downstream of the bend (as is done during operational setup of this parameter).
2) Field and field integral as a function of current were computed by interpolation using data from Schultheiss' simulations [1, 6-8]. Thus, for example,

$$
\begin{aligned}
B_{GX}^{interpolated}(I) = {} & B_{GX}^{simulated}(I_{80}^{simulated})\left(\frac{I-I_{145}^{simulated}}{I_{80}^{simulated}-I_{145}^{simulated}}\right)\left(\frac{I-I_{190}^{simulated}}{I_{80}^{simulated}-I_{190}^{simulated}}\right)\left(\frac{I-I_{210}^{simulated}}{I_{80}^{simulated}-I_{210}^{simulated}}\right) \\
& + B_{GX}^{simulated}(I_{145}^{simulated})\left(\frac{I-I_{80}^{simulated}}{I_{145}^{simulated}-I_{80}^{simulated}}\right)\left(\frac{I-I_{190}^{simulated}}{I_{145}^{simulated}-I_{190}^{simulated}}\right)\left(\frac{I-I_{210}^{simulated}}{I_{145}^{simulated}-I_{210}^{simulated}}\right) \\
& + B_{GX}^{simulated}(I_{190}^{simulated})\left(\frac{I-I_{80}^{simulated}}{I_{190}^{simulated}-I_{80}^{simulated}}\right)\left(\frac{I-I_{145}^{simulated}}{I_{190}^{simulated}-I_{145}^{simulated}}\right)\left(\frac{I-I_{210}^{simulated}}{I_{190}^{simulated}-I_{210}^{simulated}}\right) \\
& + B_{GX}^{simulated}(I_{210}^{simulated})\left(\frac{I-I_{80}^{simulated}}{I_{210}^{simulated}-I_{80}^{simulated}}\right)\left(\frac{I-I_{145}^{simulated}}{I_{210}^{simulated}-I_{145}^{simulated}}\right)\left(\frac{I-I_{190}^{simulated}}{I_{210}^{simulated}-I_{190}^{simulated}}\right)
\end{aligned}
$$

   with similar expressions for the rest of the fields and field integrals. (We remark that only 80, 145, and 210 MeV/c data were supplied and used for the GY.)
3) The lengths (the hsl, to be precise) of the GX and GQ were modified to reduce deviations according to expressions of the form

$$BL_{GX}(I) = BL_{GX}^{interpolated}(I) + \Delta l_{GX} B_{GX}^{interpolated}(I)$$
$$BL_{GQ}(I) = BL_{GQ}^{interpolated}(I) + \Delta l_{GQ} B_{GQ}^{interpolated}(I)$$

These length adjustments were applied commonly across the full excitation range.

4) The GY gap was adjusted to provide an additional free parameter according to the relations

$$B_{GY}^{interpolated}(I) = B_{GY}^{noinal\ interpolated}(I) \div g$$
$$(BL)_{GY}^{interpolated}(I) = (BL)_{GY}^{noinal\ interpolated}(I) \div g$$

in which the interpolated field (and integral) at current I has been adjusted from the "nominal" interpolated field (and integral, both established in the manner described in 2), above) through the use of a "gap factor" g representing the relative change of the dipole gap. Use of this adjustment allows modification of the required shunt dynamic range and in particularly allows us to increase the required shunt excitation away from small values at low operating momenta.

5) GX and GQ field integrals were further adjusted at full excitation only using a modeled shim. The field integrals were then taken to be

$$BL_{GX}(I) = BL_{GX}^{interpolated}(I) + \left(\Delta l_{GX} + l_{GX\ shim}\right) B_{GX}^{interpolated}(I)$$
$$BL_{GQ}(I) = BL_{GQ}^{interpolated}(I) + \left(\Delta l_{GQ} + l_{GQ\ shim}\right) B_{GQ}^{interpolated}(I)$$

These reflect an operational philosophy which low-momentum runs (≲190 MeV/c) will be performed without shims; high-momentum runs will be performed with shims installed as needed (but more on this below).

Table 3 describes the system prior to the optimization of core field and field integral. Modeled, design, and "adjusted" data, evaluated as described above, are summarized in the first three sections of the table. The allowed adjustments (GX and GQ core length, GY shunt, GY gap, GX and GQ core shim length) – not yet implemented – are detailed in the fourth section. Deviations of adjusted from design data are presented in the final section. In this analysis, the operating current (shaded blue in the "Adjusted data" section) has been set to zero the GX relative field integral deviation at each operating momentum. As noted above, this ensures we have "correctly turned the corner". The GY shunt (in the "Adjustments" section) has been set to zero the GY field deviation for each operating momentum, ensuring that the correct orbit radius occurs in the π-bend.

Inspection of the "Deviations" indicates that all is not well. Though the GX field integral is correct, the field is significantly different from design at all but full excitation. GQ fields and integrals are out of spec over the same range. The GY "runs out of shunt" – that is, even zeroing the shunt fails to correct the field – for all but the highest momenta, and, even at 190 MeV/c, the shunt will be nearly railed. The beamline performance will thus likely be poor: the beam will be badly steered and incorrectly focused.

Table 3: Anticipated endloop dipole operational performance without adjustments to lengths or gaps.

Modeled data		**GX**			**GQ**				**GY**			
E	I	B	BL	L	I	B	BL	L	I	B	BL	L
80	85.1675	2.2238	2.0512	0.9224	84.9770	2.2236	2.0012	0.9000	84.8408	2.6686	8.3806	3.1404
145	154.4485	4.0306	3.7152	0.9217	154.1385	4.0302	3.6244	0.8993	153.8040	4.8369	15.1903	3.1405
190	203.4903	5.2818	4.8607	0.9203	203.1293	5.2814	4.7417	0.8978				
210	227.2750	5.8371	5.3562	0.9176	227.2750	5.8372	5.2235	0.8949	223.8659	7.0052	22.0096	3.1419

Design data	**GX**			**GQ**			**GY**		
E	B	BL	L	B	BL	L	B	BL	L
80	2.2238	2.0403	0.9175	2.2238	1.9898	0.8948	2.6685	8.3834	3.1416
145	4.0306	3.6980	0.9175	4.0306	3.6065	0.8948	4.8367	15.1949	3.1416
190	5.2814	4.8456	0.9175	5.2814	4.7258	0.8948	6.3377	19.9105	3.1416
210	5.8374	5.3557	0.9175	5.8374	5.2232	0.8948	7.0048	22.0064	3.1416

Adjusted data		**GX**			**GQ**				**GY**			
E	I	B	BL	L	I	B	BL	L	I	B	BL	L
80	84.6900	2.2119	2.0404	0.9225	84.6900	2.2165	1.9949	0.9000	84.6900	2.6638	8.3656	3.1405
145	153.7400	4.0119	3.6980	0.9217	153.7400	4.0196	3.6149	0.8993	153.7400	4.8349	15.1840	3.1405
190	202.8000	5.2650	4.8456	0.9203	202.8000	5.2735	4.7347	0.8978	202.1713	6.3375	19.9087	3.1414
210	227.2500	5.8365	5.3557	0.9176	227.2500	5.8367	5.2230	0.8949	223.8640	7.0051	22.0094	3.1419

delta L GX	delta L GQ	shunt GY	at E	GY gap	GX shim	GQ shim	
0.0000	0.0000	0	80	1	0	0	
		0	145				**Adjustments**
		0.0031	190				
		0.0149	210				

Deviations	**GX**		**GQ**		**GY**	
E	dB/B	dBL/BL	dB/B	dBL/BL	dB/B	dBL/BL
80	-0.0053	0.0000	-0.0033	0.0026	-0.0018	-0.0021
145	-0.0046	0.0000	-0.0027	0.0023	-0.0004	-0.0007
190	-0.0031	0.0000	-0.0015	0.0019	0.0000	-0.0001
210	-0.0001	0.0000	-0.0001	0.0000	0.0000	0.0001

figure of merit
0.03281

Table 4 presents similar data after adjustments are made to the GX and GQ length (as shown in Figure 5) and the GY gap. The agreement between the adjusted and the design values is improved at all but the highest excitations. The GX field is within a factor of 2 of specification from 80 to 190 MeV/c; we note that the system is likely tolerant of this inasmuch as the associated focusing errors couple only weakly to the beam envelopes and dispersions, which are relatively small at this magnet. GQ fields and integrals are also in fair agreement with design. Of most concern is the 0.18% relative field deviation at 190 MeV/c. This may generate focusing errors that couple to the large dispersion in the GQ, but these can likely be compensated by the adjacent trim quads. Also reassuring is the improved GY shunt operability – the shunt stays reasonably far away (>½%) from its limiting values (of 0 and 3%) across the full operating range of the dipole. This operating scenario is thus likely to be satisfactory for the foreseeable future, as operation at 210 MeV/c will occur only after a full complement of three 7-cell based cryomodules becomes available.

Table 4: Anticipated endloop dipole performance following adjustments to GX and GQ length and GY gap.

Modeled data		GX				GQ				GY		
E	I	B	BL	L	I	B	BL	L	I	B	BL	L
80	85.1675	2.2238	2.0512	0.9224	84.9770	2.2236	2.0012	0.9000	84.8408	2.6686	8.3806	3.1404
145	154.4485	4.0306	3.7152	0.9217	154.1385	4.0302	3.6244	0.8993	153.8040	4.8369	15.1903	3.1405
190	203.4903	5.2818	4.8607	0.9203	203.1293	5.2814	4.7417	0.8978				
210	227.2750	5.8371	5.3562	0.9176	227.2750	5.8372	5.2235	0.8949	223.8659	7.0052	22.0096	3.1419

Design data	GX			GQ			GY		
E	B	BL	L	B	BL	L	B	BL	L
80	2.2238	2.0403	0.9175	2.2238	1.9898	0.8948	2.6685	8.3834	3.1416
145	4.0306	3.6980	0.9175	4.0306	3.6065	0.8948	4.8367	15.1949	3.1416
190	5.2814	4.8456	0.9175	5.2814	4.7258	0.8948	6.3377	19.9105	3.1416
210	5.8374	5.3557	0.9175	5.8374	5.2232	0.8948	7.0048	22.0064	3.1416

Adjusted data		GX				GQ				GY		
E	I	B	BL	L	I	B	BL	L	I	B	BL	L
80	84.9800	2.2191	2.0403	0.9194	84.9800	2.2237	1.9901	0.8950	84.4191	2.6686	8.3806	3.1405
145	154.2400	4.0251	3.6981	0.9187	154.2400	4.0329	3.6067	0.8943	153.0215	4.8367	15.1895	3.1405
190	203.5200	5.2825	4.8455	0.9173	203.5200	5.2908	4.7235	0.8928	201.1592	6.3380	19.9100	3.1414
210	228.1500	5.8566	5.3558	0.9145	228.1500	5.8563	5.2104	0.8897	222.7200	7.0050	22.0089	3.1419

delta L GX	delta L GQ	shunt GY	at E	GY gap	GX shim	GQ shim
-0.0030	-0.0050	0.0066	80	0.995	0	0
		0.0079	145			
		0.0116	190			
		0.0238	210			

Adjustments

Deviations	GX		GQ		GY	
E	dB/B	dBL/BL	dB/B	dBL/BL	dB/B	dBL/BL
80	-0.0021	0.0000	0.0000	0.0002	0.0000	-0.0003
145	-0.0014	0.0000	0.0006	0.0000	0.0000	-0.0004
190	0.0002	0.0000	0.0018	-0.0005	0.0000	0.0000
210	0.0033	0.0000	0.0032	-0.0024	0.0000	0.0001

figure of merit
0.01663

Operation at full excitation, though not immediately anticipated, can be accommodated either through compensation using trim quads (as invoked above for GQ operation at 190 MeV/c, should focusing error effects be excessive), or through the use of shims. Such a scenario is presented in Table 5, wherein the Table 4 solution is further adjusted, at full excitation only, through the use of 2.5 mm shims. It is assumed these are applied in pairs to the GQ and to the "interior" (to the endloop) pole of the GXs. The GX compensation is done in manner to allow UV operation and will discussed further below. Here, we note only that the net effect of this asymmetric correction will be to move the GX bend center ~1.25 mm toward the interior of the endloop; this is well within the nominal longitudinal alignment tolerance of a few millimeters. Shim configurations are illustrated in Figure 5.

Table 5: Anticipated performance using Table 4 solution at lower operating momenta and shimming of GX and GQ (per Figure 5) at full excitation.

Modeled data	GX				GQ				GY			
E	I	B	BL	L	I	B	BL	L	I	B	BL	L
80	85.1675	2.2238	2.0512	0.9224	84.9770	2.2236	2.0012	0.9000	84.8408	2.6686	8.3806	3.1404
145	154.4485	4.0306	3.7152	0.9217	154.1385	4.0302	3.6244	0.8993	153.8040	4.8369	15.1903	3.1405
190	203.4903	5.2818	4.8607	0.9203	203.1293	5.2814	4.7417	0.8978				
210	227.2750	5.8371	5.3562	0.9176	227.2750	5.8372	5.2235	0.8949	223.8659	7.0052	22.0096	3.1419

Design data	GX			GQ			GY		
E	B	BL	L	B	BL	L	B	BL	L
80	2.2238	2.0403	0.9175	2.2238	1.9898	0.8948	2.6685	8.3834	3.1416
145	4.0306	3.6980	0.9175	4.0306	3.6065	0.8948	4.8367	15.1949	3.1416
190	5.2814	4.8456	0.9175	5.2814	4.7258	0.8948	6.3377	19.9105	3.1416
210	5.8374	5.3557	0.9175	5.8374	5.2232	0.8948	7.0048	22.0064	3.1416

Adjusted data	GX				GQ				GY			
E	I	B	BL	L	I	B	BL	L	I	B	BL	L
80	84.9800	2.2191	2.0403	0.9194	84.9800	2.2237	1.9901	0.8950	84.4191	2.6686	8.3806	3.1405
145	154.2400	4.0251	3.6981	0.9187	154.2400	4.0329	3.6067	0.8943	153.0215	4.8367	15.1895	3.1405
190	203.5200	5.2825	4.8455	0.9173	203.5200	5.2908	4.7235	0.8928	201.1592	6.3380	19.9100	3.1414
210	227.4100	5.8401	5.3559	0.9171	227.4100	5.8401	5.2260	0.8948	222.7026	7.0045	22.0072	3.1419

delta L GX	delta L GQ	shunt GY	at E	GY gap	GX shim	GQ shim
-0.0030	-0.0050	0.0066	80	0.995	0.0025	0.005
		0.0079	145			
		0.0116	190			
		0.0207	210			

Adjustments

Deviations	GX		GQ		GY	
E	dB/B	dBL/BL	dB/B	dBL/BL	dB/B	dBL/BL
80	-0.0021	0.0000	0.0000	0.0002	0.0000	-0.0003
145	-0.0014	0.0000	0.0006	0.0000	0.0000	-0.0004
190	0.0002	0.0000	0.0018	-0.0005	0.0000	0.0000
210	0.0005	0.0000	0.0005	0.0005	0.0000	0.0000

figure of merit
0.00911

Figure 5a: Shave/shim configurations for GQ

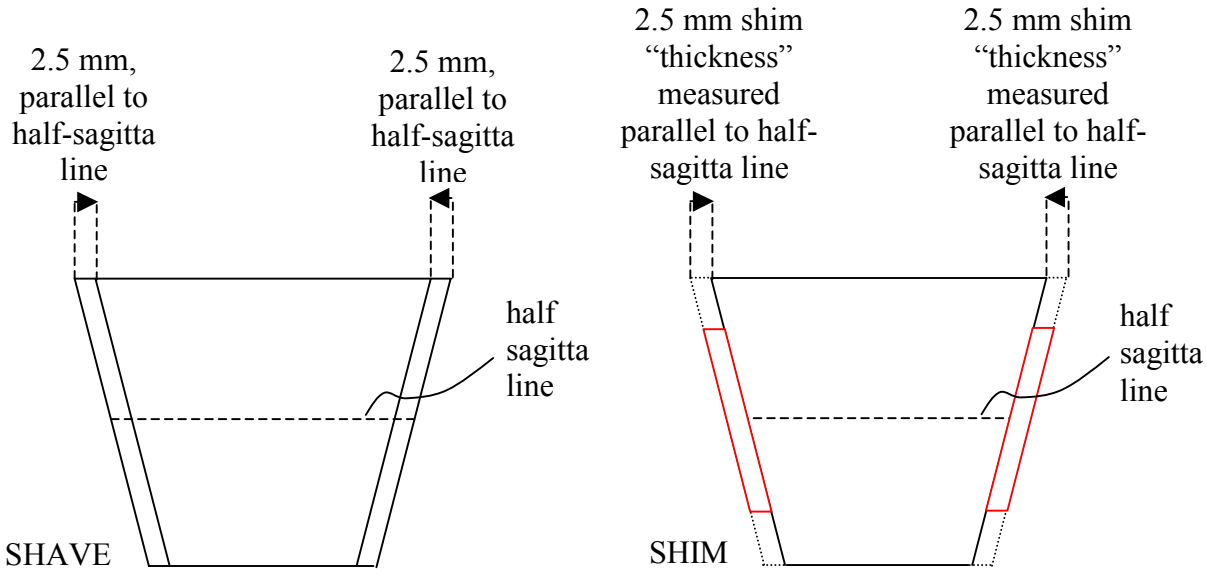

Figure 5b: Shave/shim configurations for GX

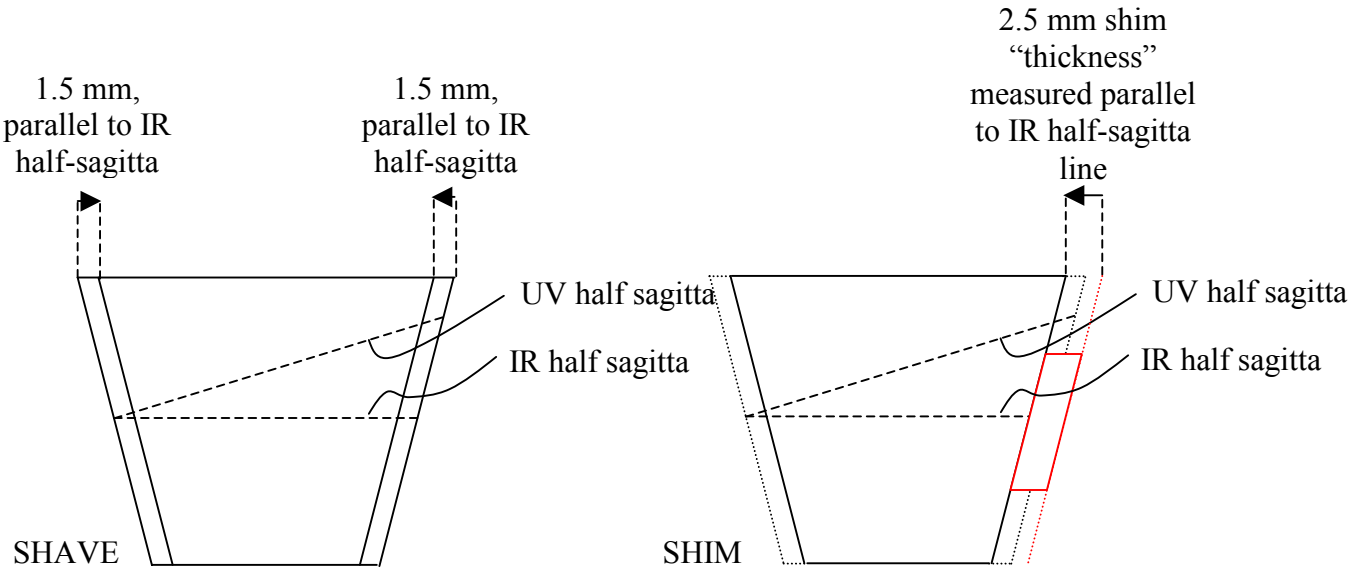

GX/UV Performance – Tracking Accuracy of Core Field/Field Integral

The GX/UV application described above has been simulated by Schultheiss [7]; results from these simulations and a comparison with design are given in Table 6. Table 7 repeats this comparison in an operational context. Operating points evaluated by interpolation are shaded lavender and are suspect (*i.e.,* should be ignored, even though not negligible). Near simulated set-points, the interpolation (which is only linear and based on simulation at just 145 and 210 MeV/c) may be regarded as more reliable and suggests that a reasonable match of core field and field integral may be achieved by shaving and shimming as in Figure 5a. We remark that the "excessive effective length" observed in simulation has as its source the aforementioned saturation of the magnet at its nominal design excitation for 210 MeV/c.

Table 6: Comparison of design values and Schultheiss' simulation results.

Property	GX – IR application				GX – UV application	
momentum (MeV/c)	80	145	190	210	145	210
design field (kg)	2.2238	4.0306	5.2814	5.8374	2.0153	2.9187
design length (m)	0.9175				0.9807	
design ∫Bdl (kg-m)	2.0403	3.6980	4.8456	5.3557	1.9764	2.8624
simulated field (kg)	2.2238	4.0306	5.2818	5.8371	2.0153	2.9188
required current (A)	85.1675	154.4485	203.4903	227.2750	154.0381	223.1454
$(I-I_{GX/IR})/I_{GX/IR}$					*-0.00266*	*-0.0182*
simulated ∫Bdl (kg-m)	2.0512	3.7152	4.8607	5.3562	1.9832	2.8723
$(\int Bdl-\int Bdl_{design})/\int Bdl_{design}$	*0.0053*	*0.0047*	*0.0031*	*0.0001*	*0.0034*	*0.0035*
effective length (m)	0.9224	0.9217	0.9203	0.9176	0.9841	0.9841
$(L_{effective}-L_{design})/L_{design}$	*0.0053*	*0.0046*	*0.0031*	*0.0001*	*0.0035*	*0.0035*

Table 7: Comparison of design, simulated, and operationally implemented fields. Blue fields are adjusted away from design and/or set operationally, lavender fields are (blindly) interpolated and are provided solely for their entertainment value.

Modeled data				GX					GQ				GY			
E	I	B	BL	I (UV)	B UV	BL UV	L	L UV	I	B	BL	L	I	B	BL	L
80	85.1675	2.2238	2.0512				0.9224		84.9770	2.2236	2.0012	0.9000	84.8408	2.6686	8.3806	3.1404
145	154.4485	4.0306	3.7152	154.0381	2.0153	1.9832	0.9217	0.9841	154.1385	4.0302	3.6244	0.8993	153.8040	4.8369	15.1903	3.1405
190	203.4903	5.2818	4.8607				0.9203		203.1293	5.2814	4.7417	0.8978				
210	227.2750	5.8371	5.3562	223.1454	2.9188	2.8723	0.9176	0.9841	227.2750	5.8372	5.2235	0.8949	223.8659	7.0052	22.0096	3.1419

Design data		GX					GQ				GY		
E	B	BL	B UV	BL UV	L	L UV	B	BL	L	B	BL	L
80	2.2238	2.0403			0.9175		2.2238	1.9898	0.8948	2.6685	8.3834	3.1416
145	4.0306	3.6980	2.0153	1.9764	0.9175	0.9807	4.0306	3.6065	0.8948	4.8367	15.1949	3.1416
190	5.2814	4.8456	2.6407	2.5897	0.9175	0.9807	5.2814	4.7258	0.8948	6.3377	19.9105	3.1416
210	5.8374	5.3557	2.9187	2.8623	0.9175	0.9807	5.8374	5.2232	0.8948	7.0048	22.0064	3.1416

Adjusted data				GX					GQ				GY			
E	I	B	BL	I (UV)	B UV	BL UV	L	L UV	I	B	BL	L	I	B	BL	L
80	84.9800	2.2191	2.0403				0.9194		84.9800	2.2237	1.9901	0.8950	84.4191	2.6686	8.3806	3.1405
145	154.2400	4.0251	3.6981	154.2400	2.0127	1.9745	0.9187	0.9810	154.2400	4.0329	3.6067	0.8943	153.0215	4.8367	15.1895	3.1405
190	203.5200	5.2825	4.8455	203.5200	2.6241	2.5743	0.9173	0.9810	203.5200	5.2908	4.7235	0.8928	201.1592	6.3380	19.9100	3.1414
210	227.4100	5.8401	5.3413	227.4100	2.9205	2.8650	0.9146	0.9810	227.4100	5.8401	5.1968	0.8898	222.7026	7.0045	22.0072	3.1419

delta L GX	delta L GQ	shunt GY	at E	GY gap	GX shim	GQ shim
-0.0030	-0.0050	0.0066	80	0.995	0	0
		0.0079	145			
		0.0116	190			
		0.0207	210			

Adjustments

Deviations		GX			GQ		GY	
E	dB/B	dBL/BL	dB/B UV	dBL/BL UV	dB/B	dBL/BL	dB/B	dBL/BL
80	-0.0021	0.0000			0.0000	0.0002	0.0000	-0.0003
145	-0.0014	0.0000	-0.0013	-0.0009	0.0006	0.0000	0.0000	-0.0004
190	0.0002	0.0000	-0.0063	-0.0060	0.0018	-0.0005	0.0000	0.0000
210	0.0005	-0.0027	0.0006	0.0009	0.0005	-0.0051	0.0000	0.0000

figure of merit
0.01628

Core field and field integral can thus be provided for all magnets to within a factor of two of tracking specifications by appropriate shaving, shimming, and operational setup. We remark that the Figure 5b shim configuration is intended to *avoid* adding length to the UV path at 210 MeV/c, thereby avoiding associated excess effective length.

Core Field Homogeneity

The core field in driver endloop dipoles is to be flat to order 10^{-4} over the working aperture to avoid phase space distortion effects, which can lead to performance limitations [Table 1, ref. 2, 3, 9]. Simulations by Schultheiss have evaluated the expected core field throughout each magnet style at various working excitations. He has further distilled these results to provide field tabulations along "straight-through" integration paths, and evaluated the field integrals along these paths to facilitate comparison to magnetic measurements. In the following, we will review his results for field and field integral characteristics for the GX in both IR and UV applications and for the GQ.

GX: IR Application – Figure 6 presents results from Schultheiss [10] for the core field in the GX dipole at full (210 MeV/c) excitation. We have overlaid circular arcs of radius 1.2, 1.15 and 1.25 m to represent, respectively, the central orbit and the inner and outer limits of the 100 kW beam stay-clear.

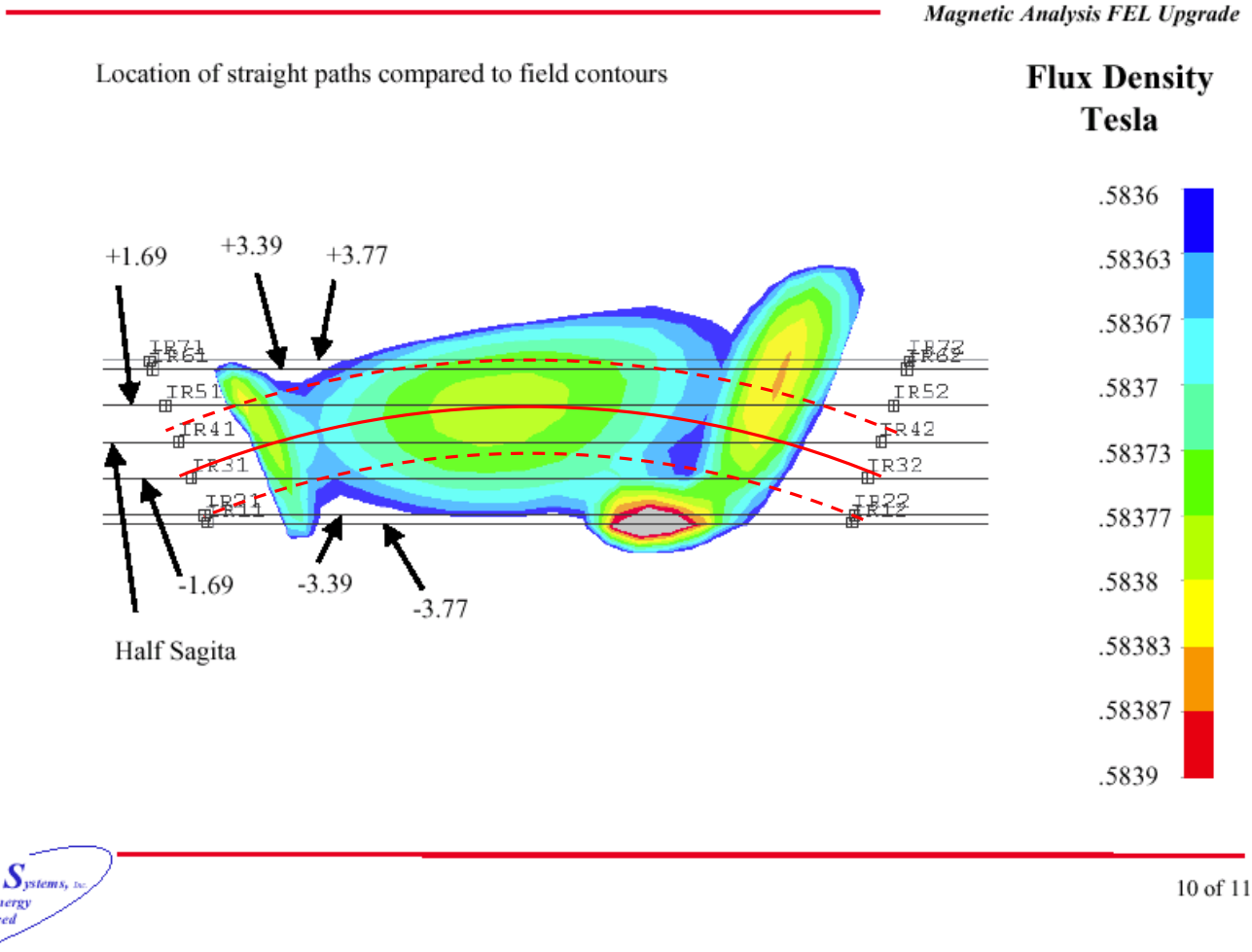

Figure 6: Schultheiss' simulation [10] of core field in GX dipole. We have superposed central orbit (solid red line) and limits of working aperture (dashed red lines – limits of 100 kW beam stay-clear).

The key feature of the field homogeneity criterion is that the field be flat *across* the beam – that is, varying only slightly in the radial direction. This precludes erroneous differential bending of the phase space, which will generate distortion and result in emittance growth. Examination of Figure 6 reveals this to be the case. Though the field varies by several 10^{-4} *along* the orbit, it changes only by a few 10^{-4} across the orbit. Provided the integrals along the various orbits match the required values (*i.e.*, assuming the "bumps average out" along each orbit), this transverse homogeneity ensures that phase space distortion and emittance degradation will be avoided. In Figure 7, we show data from Schultheiss' field map for the GX in 80 MeV operation [11], presented so as to

illustrate the field value along each of the chords in Figure 6. On this, we have projected the radial extent of the Figure 6 extent of the working aperture. Each of the red arcs superposed on the magnet data is the image of a "spoke" (each separated by 1/20th of the angle subtended by the central orbit) starting at the inner aperture limit and ending at the outer. The limit in field variation along each spoke is clearly of order a few 10^{-4}.

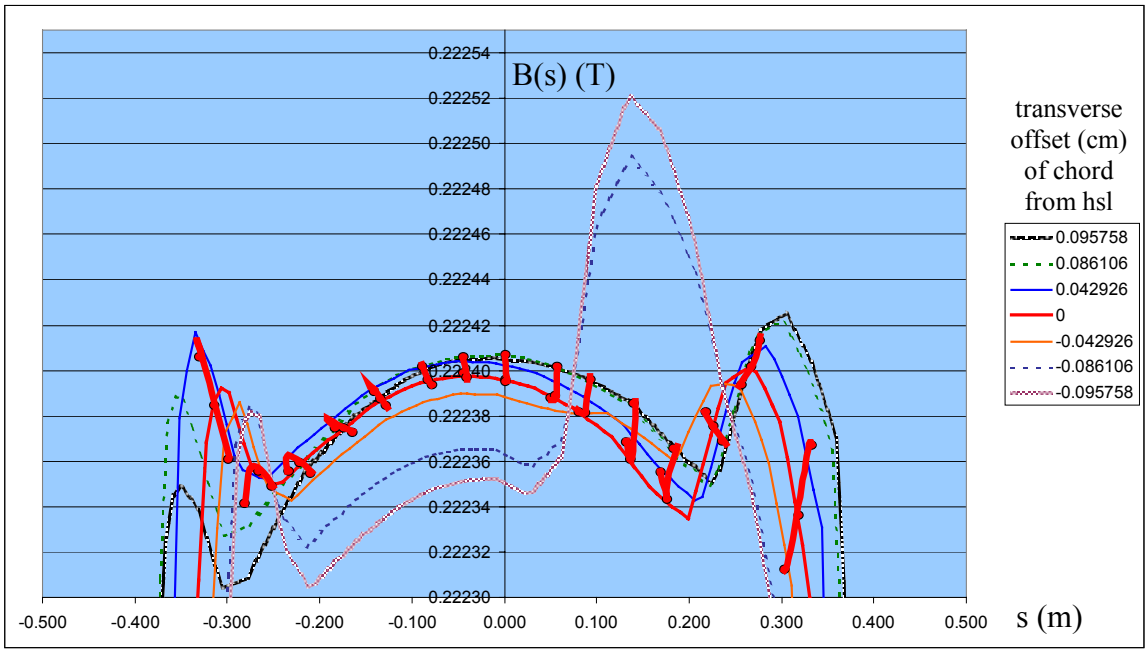

Figure 7: Radial cuts superposed on field map along chords shown in Figure 6. Field variations with transverse position are largely limited to order 10^{-4}.

In the following section, we will address the issue of the homogeneity of the field integrals; for the moment, we turn attention to use of the GX in the UV bypass and the GQ for both IR and UV applications.

GX: UV Application – Figure 8 illustrates the UV analogue to Figure 6. The central orbit (red solid arc) and limits of beam stay-clear (red dashed arcs) are superposed on a Schultheiss simulation of the GX in UV operation (here, at 145 MeV/c, [12]). As in Figure 6, the field is homogeneous in the transverse direction to the 10^{-4} level

GQ: IR and UV Application – Figure 9 illustrates the GQ analogue to Figures 6 and 8. The central orbit (red solid arc) and limits of beam stay-clear (red dashed arcs) are superposed on a Schultheiss simulation of the GQ as excited for either IR or UV operation at 210 MeV/c, [13]. The very large field volume of interest is due to a dispersion of ~1.6 m in this dipole; at nominal IR/UV operating parameters ($\delta p/p$~10%), this corresponds to a dispersive spot size of 16 cm, which, when combined with 4 cm working aperture and almost 9 cm of sagitta leads to a beam stay-clear of 30 cm. Even wider is the 38+ cm stay-clear of interest for 100 kW operation. This will allow

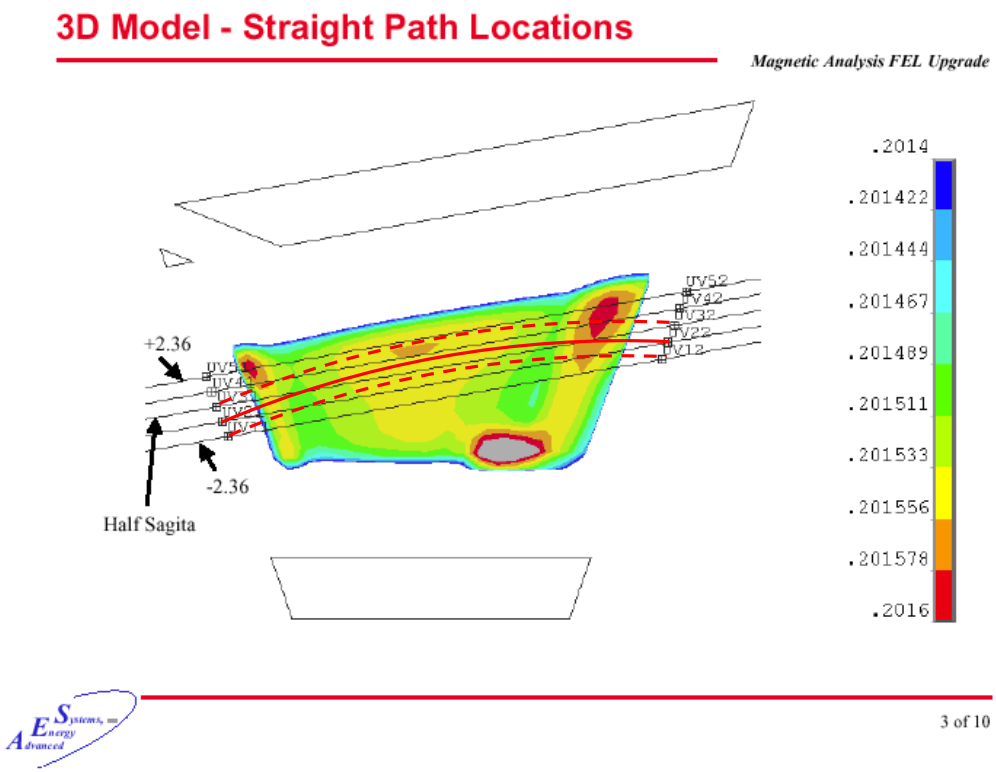

Figure 8: Schultheiss' simulation [12] of core field in GX dipole when energized for UV operation at 145 MeV/c. We have superposed central orbit (solid red line) and limits of working aperture. Field intensities are in Tesla each color gradation is of order 10^{-4} in variation from the adjacent value. The field is radially homogeneous to order 10^{-4} throughout.

momentum spreads of order 15% (dispersed spot sizes of 25 cm) while still providing 4 cm working aperture and the nominal sagitta allowance. As in the previous cases, the field is radially homogeneous to the 10^{-4} level for the nominal 10 kW operating parameters and not seriously degraded (a few to several 10^{-4} variation) at even 100 kW.

Field Integral Uniformity

In this discussion, we must recall that the homogeneity requirements on the core field are driven by a need to avoid phase space distortion and emittance dilution [2,3]. Thus, the core field must, first, be flat to 0.1 ppt radially *across* the beam at any central orbit azimuthal displacement through the magnet, and, second, the field integral along a test trajectory must match the intended design value to 0.1 ppt. We have seen above that the first requirement is well met by the Schultheiss design. We now consider the second requirement, which does not demand that the field exhibit variations of less that 0.1 ppt

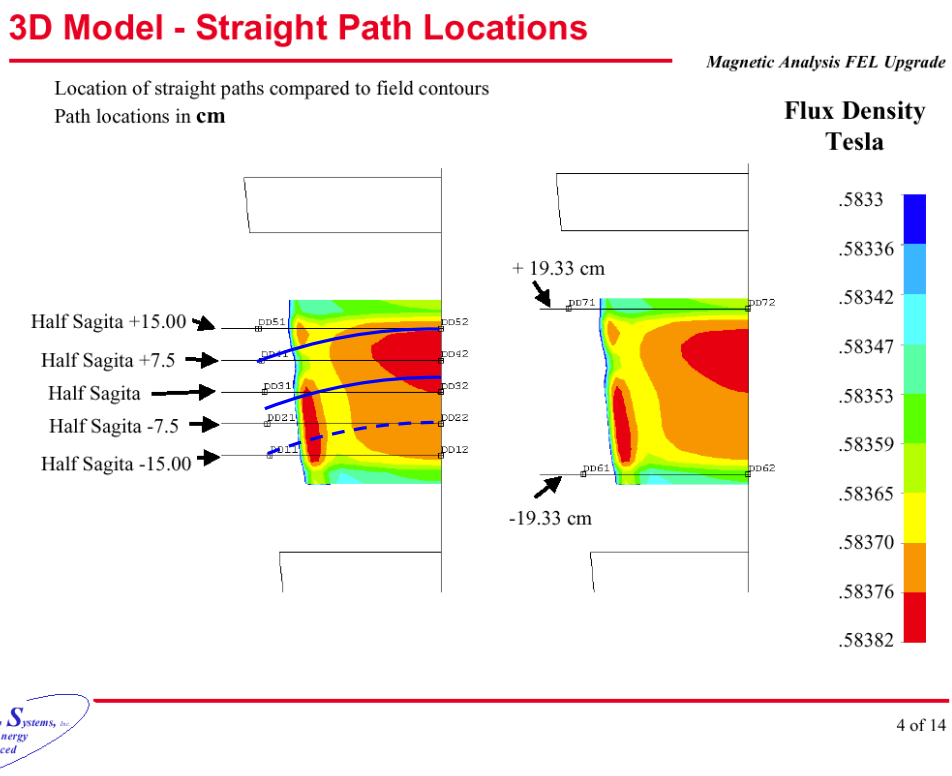

Figure 9: Schultheiss' simulation [13] of core field in GQ dipole when energized for either IR or UV operation at 210 MeV/c. The left figure illustrates the limits of the working aperture for nominal (10 kW) operation, the map on the right shows the limits for 100 kW operation. Each color gradation represents a deviation of order 10^{-4} of the core field. The nominal operating volume is very uniform, and the field remains flat to better than 10^{-3} over even the very large 100 kW working aperture. We have superposed the central orbit (solid blue line) and limits of the 10 kW working aperture (dashed blue line) on the left figure.

along the direction of longitudinal motion. It simply constrains the *integral* to this level; longitudinal variations from design well beyond the 10^{-4} level are tolerable, provided the "bumps average out". Given the core field homogeneity described above, it is in fact expected that field integrals along the various relevant trajectories *will* meet the Table 1 specification.

It is not, however, possible to directly measure these field integrals (along the circular arc-shaped orbits) with the available test apparatus, inasmuch as it is configured to characterize all of a variety of magnet styles. The magnet measurement system therefore evaluates "straight-through" field integrals, which sample field regions not included in the working aperture. Given the previously described transverse and longitudinal variation of the core field, the measured integrals therefore may (or may not!) meet the 10^{-4} field flatness specification appropriate to the actual beam working aperture. In this section, we review Schultheiss' results for straight through field integrals and attempt to put them in a context that will allow us to anticipate and properly interpret magnet test stand results for the GX and GQ magnets and to make a ready comparison to specification.

Figure 10 presents a rearrangement of the GX data in Figure 7, with the projections of the central orbit (solid black) and limits of working aperture (dashed black) connected azimuthally. It is clear that field variations amongst these fiduciary paths are at the 10^{-4} level, so that deviations amongst integrals along trajectories lying within these paths will also be at this level. In contrast, Figure 11 presents deviations of simulated field integrals evaluated along the straight-line ("measured") paths of Figure 6 from ideal values (established with formulae given above). The variation is clearly well beyond the desired 10^{-4} level. We cannot, therefore, expect rotating coil measurements to exhibit the specified field flatness.

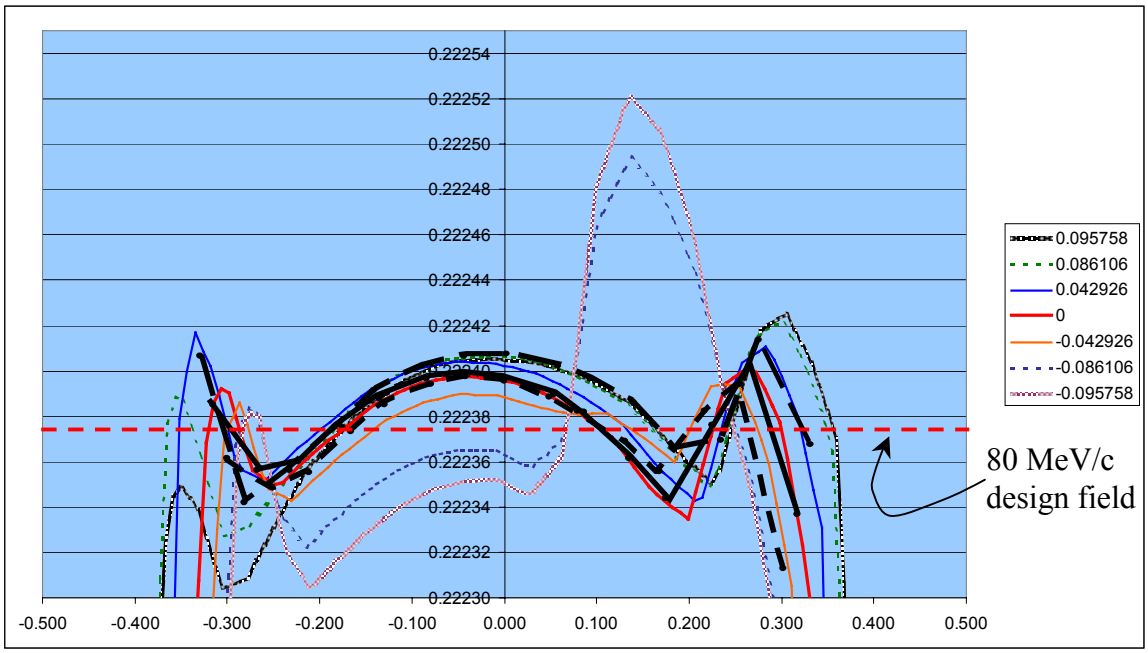

Figure 10: GX field map for 80 MeV IR excitation, with field along central orbit (solid) and extrema of beam stay-clear (dashed) highlighted.

This is, however, not unexpected. Due to the large orbit sagitta and field volume, the magnet gap was adjusted locally to flatten the field over the beam stay clear [14]. This produces local peaks and valleys in the field map (see, for example, the "silver" peak in the lower right hand corner of the field map in Figure 8, corresponding to the peak in the solid rose and dashed green curves in Figure 10, at offsets of –0.095758 m and –0.086106 m, respectively) that will be seen by rotating coil measurements but will not be experienced by the beam. Figure 11 shows the variation in field integrals through the GX as a function of offset from the hsl at a variety of excitations. Though not within specification for the working aperture, the variation is modest and as noted, the beam does not enter the region generating the deviation from specification. These observations and comments apply to both GX and GQ, though given the more regular GQ geometry, the effect should not be as evident. (See Figure 12, which presents the GQ data corresponding to the GX information shown by Figure 11).

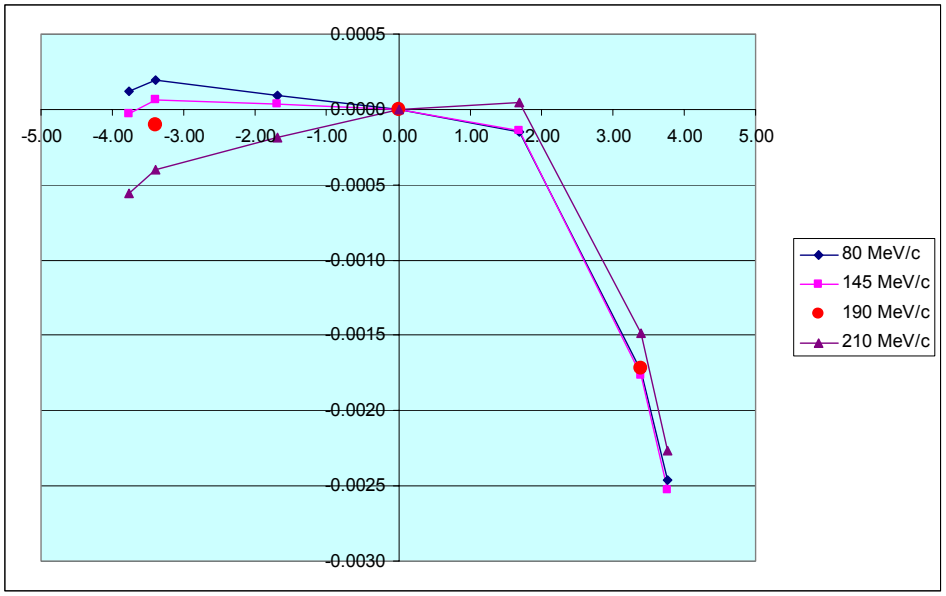

Figure 11: Deviation in "straight through" GX field integral from ideal vs. offset from hsl at several excitations. We have suppressed an excitation dependant DC offset, equivalently assuming a length adjustment such as that discussed above. Data from Schultheiss spreadsheets and an unpublished report [15].

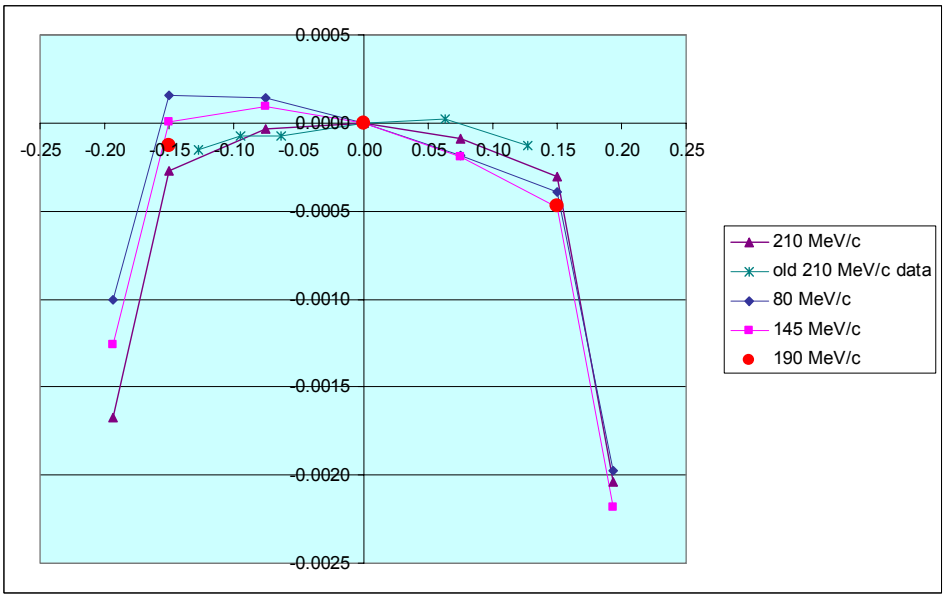

Figure 12: Deviation in "straight through" GQ field integral from ideal vs. offset from hsl at several excitations. We have again suppressed the excitation dependant DC offset, equivalently assuming a length adjustment such as that discussed above. Data from Schultheiss unpublished reports and spreadsheet [16].

Conclusions

The preceding discussion demonstrates that the GX, GQ, and GY designs should meet, or be easily modified to meet, the principle design requirements presented in Table 1. Two particular issues requiring attention are the excitation dependent effective length and the transverse variation in "straight through" field integral. With respect to the former, proper adjustment of the yoke length with appropriate use of shims at the highest excitations will give adequate performance across the full 80-210 MeV/c excitation range. As to the latter, we have seen that the field homogeneity appears adequate over the working aperture (that used by the beam), but variations in measured integral well beyond specification are likely to be encountered during rotating-coil based magnetic measurements. Proper interpretation of these results, together with mapping using Hall probes should certify satisfactory performance of each magnet.

Results of this study also suggest a similar evaluation of GW performance (either in simulation or on the test stand) would be prudent.

The spreadsheets used in this note are available to the curious or incautious from the first author.

References

[1] T. Schultheiss has provided numerous documents presenting results of simulations of the performance of GX, GQ and GY dipoles. We make reference to some of these in subsequent citations. We will, in addition, directly cite specific documents when quoting results.

[2] See, for example, D. Douglas, "Comments on Driver Dipole Good Fields", JLAB-TN-96-066, 5 December 1996 and references therein; D. Douglas and B. C. Yunn, "The Effect of Field Inhomogeneities in Upgrade Injection Line Dipoles, JLAB-TN-01-016, 23 March 2001; D. Douglas, "Some Features of the FEL Upgrade π-Bends", JLAB-TN-01-024, 14 May 2001; D. Douglas and G. Biallas, "GY Field Homogeneity Evaluation", JLAB-TN-01-042, 22 August 2001; D. Douglas, "The Effect of Field Inhomogeneities In or Near the IR Upgrade Driver Compaction Management Elements", JLAB-TN-01-053.

[3] D. Douglas, "Error Estimates for the IR FEL Transport System", CEBAF-TN-96-035, 15 July 1996.

[4] D. Douglas, "Some Features of the FEL Upgrade π-Bends", *op. cit.*; D. Douglas and G. Biallas, "GY Field Homogeneity Evaluation", *op. cit.*

[5] T. Schultheiss, "GQ Magnet Configuration at Excitations of 210, 145, and 80 MeV/c", unpublished report, 2/07/2002; T. Schultheiss, "GX/GQ Magnets at 190 MeV/c excitation", unpublished report, 2/27/2002.

[6] T. Schultheiss, "GX Magnet Configuration with added evaluation lines, 210, 145, 80 MeV/c IR", unpublished report, 2/14/2002; T. Schultheiss, "GX/GQ Magnets at 190 MeV/c excitation", unpublished report, 2/27/2002.

[7] T. Schultheiss, "GX Magnet Configuration Energized for UV at 223.1454 amps 1/2 Field (210/2 MeV/c) Wider Bounds", unpublished report, 2/5/2002; T. Schultheiss, "GX Magnet Configuration Energized for UV at 154.0381 amps 1/2 Field (145/2 MeV/c) Wider Bounds", unpublished report, 2/8/2002.

[8] T. Schultheiss, "GX Magnet at Excitations for Beam Momentum of 210 MeV/c, 145 MeV/c, and 80 MeV/c", unpublished report, 2/14/2002.

[9] D. Douglas, "A Magnet Field Quality Limitation on ERL Performance", JLAB-TN-02-002, 10 January 2002.

[10] T. Schultheiss , "GX Magnet Configuration wider evaluation lines 210 MeV/c IR", unpublished report, 2/6/01.

[11] GX 80 MeV field map data from T. Schultheiss in gx.wide.ir.80.dd.xls

[12] T. Schultheiss, "GX Magnet Configuration Energized for UV at 154.0381 amps 1/2 Field (145/2 MeV/c) Wider Bounds", *op. cit.*

[13] T. Schultheiss, "GQ Magnet Configuration at Excitations of 210, 145, and 80 MeV/c", *op. cit.*

[14] T. Schultheiss *et al.*, to appear in the proceedings of FEL2002.

[15] Spreadsheets "gx.wide.ir.80.dd.xls", "gx.wide.ir.145.dd.xls", "gx.wide.ir.210.dd.xls", and T. Schultheiss, "GX/GQ Magnets at 190 MeV/c excitation", *op. cit*.

[16] T. Schultheiss spreadsheet "GQ.Dave.Douglas.12.17.01.xls"; reports "GQ Magnet Configuration at Excitations of 210, 145, and 80 MeV/c", *op. cit.* and "GX/GQ Magnets at 190 MeV/c excitation", *op. cit*.